Assessment water balance through different sources of precipitation and actual evapotranspiration

Arthur Kolling Neto (arthur.kolling@hotmail.com)
Universidade Federal de Viçosa https://orcid.org/0000-0001-6552-7282
Rayssa Balieiro Ribeiro
Fernando Falco Pruski

Research Article

Keywords: remote sensing, spatial data, management and planning, water resources

Posted Date: April 18th, 2022

DOI: https://doi.org/10.21203/rs.3.rs-1443692/v1

Abstract

Understanding the processes related to the water circulation in the watershed is essential for the development of hydrological studies, estimates of water availability and improvements in the management and planning of water resources. In this regard, the objective of this work was to evaluate the water balance (WB) behavior, resulting from the combination of precipitation (PPT) and actual evapotranspiration (ETR) from different methodologies, concerning the representativeness of the physical and climatic conditions of the watershed. For this purpose, four sources of precipitation data (IMERG, TMPA, TerraClimate and IDW interpolation of the data from rain gauge stations) and four from actual evapotranspiration (MOD16, GLEAM, MOD16rsp and TerraClimate) were considered to estimate the water balance in the Paraguaçu river watershed. The precipitation products were analyzed by means of statistical and physical analysis and the ETR products were evaluated according to the spatial distribution and magnitude of the values along the watershed. Finally, the assessment of the water balance was carried out considering the representativeness along the watershed. The results indicated that the variables (PPT_{TC} and ETR_{TC}), obtained from the TerraClimate database, showed better sensitivity to variations in the spatial distribution of each region, characterizing the orographic effect and the semi-arid climate, leading to the best performances and the best combination for the water balance (WB_{TC_TC}). Therefore, WB_{TC_TC} was the most representative variable of water circulation conditions in the watershed.

1. Introduction

Knowledge of the hydrological behavior of a watershed is extremely important for the management of water resources (EDUARDO et al. 2016). Therefore, it must encompass the hydrological processes together with its particularities and support the understanding about the water balance and, mainly, the precipitation and evapotranspiration variables (HAYASHI et al. 2016).

The analysis of the water balance in the hydrological cycle is essential for the representation of water resources in different regions of the world (MOHEBZADEH and FALLAH, 2019), enabling the assessment of the variation in the amount of water stored (surface and underground) and the respective hydrological processes (precipitation, runoff and evapotranspiration) over time (FILL et al. 2005). The water balance is a valuable tool for the correct assessment of the availability of water resources in a region, allowing the characterization of the spatial and temporal variability of the hydrological regime (NANDI and MANNE, 2020).

Precipitation and evapotranspiration are the main components of the hydrological cycle (HUFFMAN et al. 1997), they characterize the inputs and outputs of water and determine water availability on the planet (LONG et al. 2014). In this regard, obtaining reliable estimates of these variables adds greater robustness to the results of hydrological studies and are of vital importance to ensure a better representation of the water balance in the watershed (RIBEIRO, 2020).

Estimates of precipitation and evapotranspiration on large spatial scales are still challenging due to the high heterogeneity of the characteristics of the Earth's surface (ROUHOLAHNEJAD FREUND et al. 2020). They mainly affect evapotranspiration, which depends on the availability of water, topography, vegetation cover, soil properties, and climate variability (GASH, 1987; FRIEDL, 1996; JANOWIAK et al. 1998). In addition, the low density of instruments that measure these variables, makes the space-time monitoring more difficult, can cause great uncertainty in more remote regions and constitutes an obstacle for many hydrological studies (FISHER et al. 2017; LELIS et al. 2018).

Remote sensing has become an important alternative to overcome the limitations in the information-gathering process (SKOFRONICK-JACKSON et al. 2017). These sensors are capable of performing direct and indirect measurements of almost all components of the hydrological cycle, with different spatial and temporal resolutions and, in addition, capable of providing information for the management of water resources and monitoring the evolution of hazards and their impacts (LETTENMAIER et al. 2015; MCCABE et al. 2017). However, for the best use of the information generated, it is necessary that the data obtained be evaluated (SIRISENA et al. 2020).

The evaluation of remote sensing data, or spatial data, as an alternative to hydrological data can still present many challenges, such as choosing the best database of estimated variables in regions with outstanding characteristics, such as humid regions (MOREIRA et al. 2019b) or semi-arid (RAMOELO et al. 2014; RIBEIRO, 2020). Satellite missions provide a promising and cost-effective way to estimate the individual components of the hydrological cycle, however when combined they do not close the water balance due to uncertainties in the hydrological datasets (ZHANG et al. 2018).

Sheffield et al. (2009) found that the high polarization in satellite precipitation was the main factor in the non-closure of the water balance in the Mississippi River basin, in the United States of America (USA). Gao et al. (2010) also concluded that the closure of the water balance in 13 major continental rivers in the USA was not achieved mainly due to biases in precipitation and evapotranspiration. And Moreira et al. (2019b) verified that the great uncertainties in the estimates of the precipitation and evapotranspiration variables and the low availability of measured data contributed to the non-closure of the water balance in the Brazilian Pantanal region.

In Brazil, the combination of rainfall measured at rain gauge stations associated with real evapotranspiration from satellite products (MOD16, GLEAM) generated negative values in the water balance of semi-arid regions (RIBEIRO, 2020). In this sense, it is believed that precipitation from remote sensing products (TMPA, IMERG or TerraClimate) can be an alternative to solve this problem. In addition, it is noteworthy that the TerraClimate precipitation and evapotranspiration data in Brazil are still poorly explored.

Closing the water balance is still a challenge and the refinement of information on the variation of its components has been an alternative to obtain better estimates (MOREIRA et al. 2019b). Considering that the information from remote sensing and spatial databases can lead to the process of obtaining more representative hydrological variables, the analysis of these products is extremely important. In this regard,

the objective of this work was to evaluate the behavior of the water balance resulting from the combination of precipitation and actual evapotranspiration, coming from different methodologies, concerning the representativeness of the physical and climatic conditions of the watershed.

2. Data And Methods

2.1 Study area

The Paraguaçu river watershed (Fig. 1) is in the Bahia state, between parallels 11º11'S and 13°42’S, meridians 38°48’W and 42°01’W, and an area of 54,877 km² (MEDEIROS, 2003). This watershed is the most important in the state, being responsible for supplying 60% of the population of the metropolitan region of Salvador, which is currently the fourth largest city in Brazil. Figure 1 shows the map with the location of the Paraguaçu river watershed and stream and rain gauge stations selected, respectively, in the Paraguaçu river watershed.

According to the Köppen climate classification, the Paraguaçu River watershed presents three types of climates: semi-arid climate (BSh), predominant in the central part of the watershed; dry sub-humid climate (Aw), in the upper part of the watershed, in the Chapada Diamantina region; and humid sub-humid climate (Af), in the lower part of the Paraguaçu River watershed (GENZ et al. 2012). The rainy season stretches from November to January and the annual precipitation ranges from 1600 mm to 400 mm. The predominant biome is the Caatinga, with seasonal tropical forest fragments and the relief varies from flat to mountainous with agriculture limitations (CARELLI and SANTO, 2016).

The headwaters of the Paraguaçu River are located on an altitude of approximately 1,200 m, and travels about 500 km to its mouth (CARELLI and SANTO, 2016). Due to its length, the Paraguaçu River is divided into three parts: High Paraguaçu, a stretch upstream from the Santo Antônio River confluence; Medium Paraguaçu between the mouth of Santo Antônio and the Pedra do Cavalo dam and Low Paraguaçu, a stretch downstream of the dam (SOUSA et al. 2016). Despite its economic relevance, this watershed is part of the Bahia semi-arid region, which is a critical area in terms of water resource management, and it is highly vulnerable to droughts. Figure 2 shows the map of the types of climates in the Paraguaçu river watershed.

2.2 Database

Figure 3 shows the flowchart with the steps covered in the methodology of this study.

Data from historical series of stream gauging stations inserted in the watershed and rain gauge stations located in the interior and within a radius of 50 km around it, were acquired from the website of the National Water and Basic Sanitation Agency (ANA). In addition to the data obtained in the rain gauge stations, precipitation data from the TerraClimate database were also used; and actual evapotranspiration data from different remote sensing products.

Fourteen stream gauging stations and forty-one rain gauge stations were selected with data consisting up to the year 2013. The base period was defined between 1972 and 2013, and consists of stations that contained 95% of the annual data and defined with a 20 years interval. The process of choosing the rain gauge stations was based on the fact that they have series with 20 years of data, corresponding to approximately 50% of the base period.

2.3 Precipitation

The mean annual precipitation spatialization, registered in the pluviometric stations, was done by the weighting of the inverse of the squared distance (IDW), considering the power value equals to 2. The precipitation data of TerraClimate uses climatically aided interpolation, combining high-spatial resolution climatological normals from the WorldClim dataset, with coarser spatial resolution, but time-varying data from CRU Ts4.0 and the Japanese 55-year Reanalysis (JRA55). The TerraClimate data set, have monthly temporal resolution and spatial resolution of approximately 1/24° (4 km) (ABATZOGLOU et al. 2018). According to the availability of precipitation data, images were obtained from 1972 to 2013, aiming to make them compatible with the information from the data period of the rain gauge stations.

The precipitation data from TRMM Multi-Satellite Precipitation Analysis (TMPA/3B42) L3 V7 is the result of the combination of two products, the 3-hour estimate of the 3B42-v7 algorithm and the precipitation observed by rain gauges from the Global Precipitation Climatology Center (GPCC) and CAMS (Climate Assessment and Monitoring System). This product has a spatial resolution of 0.25º (~ 27.5 km) and a temporal resolution of 1 month (HUFFMAN et al. 2007). The images were obtained on a monthly basis, of the period from 1998 to 2013, according to the availability of TRMM data in the annual interval defined in the base period.

The Integrated Multi-Satellite Retrievals (IMERG) V06 for mission GPM (Global Precipitation Measurement) is the unified U.S. algorithm that provides the multi-satellite precipitation product for the U.S. GPM team. The IMERG system is run twice in near-real time and the data have spatial 0.1° (~ 10 km) and temporal resolution of 1 month (HOU et al. 2014). Considering the base period (1972–2013), images were gotten on a monthly basis, for the period from 2000 to 2013.

2.3.1 Evaluation of precipitation values

The precipitation estimates of the different sources of information were evaluated by the spatial behavior along the watershed and by the application of statistical metrics.

For data from remote sensing products and the spatial database, the specific values of precipitation were compared with the values of rain gauge stations, using the point to pixel method, based on the geographical coordinates of each pixel (TEODORO et al. 2020). For the precipitation data interpolated with IDW, specific values were obtained through cross-validation using the k-fold method.

To evaluate the values obtained by the point to pixel and k-fold methods, the following statistical metrics were used: root-mean-square error (RMSE) (Eq. 1), which calculates the mean of the squares of the

deviations between the observed and estimated values, the mean absolute error (MAE) (Eq. 2), which is the mean of the absolute errors made by the estimate that has the same weight for the errors between the estimated values compared to the observed values (FOX, 1981) and the percent bias (PBIAS) (Eq. 3), which assesses the average tendency of the simulated data to be larger or smaller than the observed data (GUPTA et al. 1999).

$$RMSE = \sqrt{\frac{1}{n}\sum \left(E_i - O_i\right)^2} \quad (1)$$

$$MAE = n^{-1} \sum_{i=1}^{n} | E_i - O_i | \quad (2)$$

$$PBIAS = \left[\frac{\sum_{i=1}^{n} \left(E_i - O_i\right) 100}{\sum_{i=1}^{n} (O_i)} \right] \quad (3)$$

where: O_i = observed value of the dependent variable i; E_i = estimated value of the dependent variable i; n = number of observations.

2.4 Actual evapotranspiration

The actual evapotranspiration (ETR) was obtained for the watershed using the remote sensing products: MOD16 from the TERRA satellite MODIS sensor (Moderate Resolution Imaging Spectroradiometer), GLEAM (Global Land Surface Evaporation: The Amsterdam Methodology) and the TerraClimate database. To verify the influence of spatial resolution on the behavior of the ETR, the MOD16 product data was made compatible with the GLEAM product cell size.

The data from the MOD16 product, developed by Mu et al. (2007) and improved by Mu et al. (2011), estimate the actual evapotranspiration based on the Penman-Monteith equation. In addition, it provides information with spatial resolution of 1 km^2 and temporal resolution of 8 days (MOD16A2), for the period from 2000 to 2014 (LIAQAT and CHOI, 2017). Therefore, given the availability of MOD16 data for the defined base period, images from 2000 to 2013 were selected.

The actual evapotranspiration estimated by the GLEAM product uses the Priestley and Taylor equation. Images were obtained on a monthly scale, with a spatial resolution of 0.25 °, on its most recent version, model (v3) (MIRALLES et al. 2011; MARTENS et al. 2017) for the period from 1980 to 2013.

The TerraClimate data set build monthly surface water balance information using a modified Thornthwaite-Mather climatic water balance model. Its data have monthly temporal resolution and spatial resolution of 1/24º and it is updated regularly (ABATZOGLOU et al. 2018). TerraClimate actual evapotranspiration images were obtained for the period from 1972 to 2013.

2.5 Water balance

The water balance (WB) of the watershed was calculated from the usual subtraction of the flow between precipitation and the ETR, considering the combination of the different, totaling 16 combinations. In order to guarantee the overlapping of the images in the constitution of the water balance (WB), the size of the pixels and the projections of the reference system of the precipitation and ETR images were made compatible. The water balance time scale was defined according to the interval of precipitation data.

Considering long-term measurements (precipitation and REE), it was assumed that water storage in the soil is constant, so that fluctuations in these amounts become insignificant in the water balance. The evaluation of the water balance maps obtained was carried out according to the analysis of the spatial distribution and the magnitude of the values along the watershed.

3. Results And Discussion

3.1 Precipitation

Figure 4 shows the precipitation maps from the remote sensing products IMERG (2000–2013), TMPA (1998–2013), TerraClimate database (1972–2013) and data measured from the rain gauge stations and interpolated with IDW (1972–2013).

The IMERG product (PPT_{IMERG}) (Fig. 4a) has a behavior characterized by smoothed regions in terms of the variation of precipitation, with a decrease from southwest to northeast, predominance of values below 620 mm and a gradual increase in values in the southeast region, where it reaches its maximum value. One of the reasons for this variation is due to the proximity to the coast, which leads to greater values of precipitation, while in the central region of the watershed, which is characterized by the semi-arid climate, the smallest values are distributed (TANAJURA et al. 2010; SOUSA, 2016). In addition, this trend was also verified by the other analyzed products.

For the TMPA product (PPT_{TMPA}) (Fig. 4b) the spatial variation rate is more abrupt than for the PPT_{IMERG}, with a continuous trend of precipitation decay from the southwest to the northeast region. Furthermore, due to the spatial resolution of the TMPA product (pixel size), there are abrupt variations between adjacent cells in the image, visually consisting of the most discrepant behavior when compared to the other maps.

The IMERG and TMPA products demonstrate convergent performance in predicting estimates and show a tendency to behave similarly, since GPM is the successor to the TRMM mission. In corroboration, other studies also state that the performance of both is similar (SOUSA, 2016; LELIS et al. 2018), but also that they suffer interference from the region in which they are used in or from the predominant type of precipitation (SERRÃO et al. 2016; ZHOU et al. 2015). In this regard, it is clear that the TRMM has greater sensitivity to variations in regional conditions, which can be explained by its validation with the precipitation recorded in situ (SERRÃO et al. 2016).

According to Yang and Nesbitt (2014) and Dinku et al. (2011), the manifestation of high values of TRMM can be attributed, particularly, to the performance of product estimates in regions with orographic rainfall, which occur due to the influence of the relief, where the air that encounters, a physical barrier is forced to rise and condenses, which can cause heavy and massive rainfall in the highest altitude area (HOUZE, 2011). Another explanation for the sharp rise of values in the western region of the watershed can be attributed to the TRMM's own prediction characteristics in the face of sudden changes in precipitation in specific locations. This effect was also mentioned in other studies and associated with the tendency to overestimate precipitation (YANG and NESBITT, 2014).

It is noted that the data from TerraClimate (PPT_{TC}) (Fig. 4c) and the data interpolated with IDW (PPT_{IDW}) (Fig. 4d) do not maintain a continuous gradient in precipitation values, presenting a range of greater magnitude in the western part of the watershed and more smoothed variations in the other regions. Tanajura et al. (2010) and Sousa (2016) state that the orographic effect, which covers the Chapada Diamantina region (west of the watershed), provides above-average rainfall in regions with a semiarid climate (rates that exceed 1000 mm $year^{-1}$). Only the PPT_{TC} and PPT_{IDW} variables produced estimates with this order of magnitude for the western region (1060 mm $year^{-1}$ and 1050 mm $year^{-1}$, respectively).

The recording of precipitation variations from the TerraClimate data (PPT_{TC}) has good sensitivity, consolidating the transition of spatial variation more clearly, which tends to accompany the watershed relief. The PPT_{IDW}, on the other hand, is represented by the so-called “bull’s eyes” and has greater definition regarding the magnitude variations in the western part the watershed. They are similar trends obtained by different products, where each one of them has its uniqueness.

Typically, the presence of the so-called “bull’s eyes” is attributed to the lack of measuring instruments, causing the formation of concentric surfaces around the rain gauge stations, as occurs in the western region of the watershed. In addition, the northeastern region of the watershed stands out, due to the absence of rain gauge stations in the interpolation with IDW, extrapolations were generated with greater values for the water balance in the semiarid region (Fig. 4).

Despite the fluctuations inherent to the different sources of precipitation, it is clear that, except for the PPT_{IMERG}, the other precipitation estimates were more sensitive to magnitude variations and spatial distribution that occurred in the watershed. Among these, it is noteworthy that PPT_{IMERG} and PPT_{TMPA} showed similar behaviors. Likewise, the variables PPT_{TC} and PPT_{IDW} were the most similar ones and also similar to the results described in other studies about the behavior of the rainfall regime in the Paraguaçu river watershed (SOUSA, 2016; TANAJURA et al. 2010).

In addition to the proximity of the precipitation estimates magnitude in the western region of the watershed, the variables PPT_{IDW} and PPT_{TC} also show equivalent spatial behavior. It is also added that the information on the TerraClimate database fully covers the base period corresponding to the rainfall considered in the study (1972 to 2013) and, therefore, may have contributed to a greater similarity of the PPT_{IDW} results.

Regarding the precipitation qualitative analysis, it appears that the precipitation amplitude variation in the watershed estimated by the four methods is smaller than the amplitude of the observed data from the rain gauge stations. In addition, the annual amplitude of the IMERG (542 to 1151 mm) and TMPA (566 to 1182 mm) products indicated the smallest ranges of variation among the products studied, with a reduction of 804 and 773 mm, respectively, in the maximum values regarding the data from rain gauge stations. The variation range corresponded to 38.4% and 38.8%, respectively, of the value of the observed data variation range.

In essence, with regard to the magnitude of the rainfall analyzed in Fig. 4, it is observed that the PPT_{IDW} was the one that produced the greatest amplitude (1379 mm $year^{-1}$) and, in contrast, the PPT_{IMERG} generated the smallest (611 mm $year^{-1}$). Furthermore, when verifying the mean annual precipitation value, it was noted that the lowest value was recorded by PPT_{TMPA} (682 mm $year^{-1}$), while the highest was also obtained by PPT_{IDW} (743 mm). Valério and Fragoso Junior (2015) also found a value similar to the one obtained by PPT_{IDW}, for the same watershed, using the data period from 1960 to 1990. Although, PPT_{IDW} generated the highest mean value compared to the other estimates, when compared with the mean precipitation value of the rain gauge stations (802 mm), it is noted that it was 7.4% smaller.

Table 1 shows the results of the statistical indexes (MAE, RMSE and PBIAS) used to compare the results of the precipitation values obtained by the different remote sensing products, regarding the precipitation of each rain gauge station in this study.

Table 1
Performance indices result for the rainfall estimates between gauge and IMERG, TMPA, and TerraClimate

Indexes	PPT_{IDW}	PPT_{TC}	PPT_{TMPA}	PPT_{IMERG}
MAE (mm/h)	135,10	85,91	155,14	172,87
RMSE (mm/h)	135,51	120,39	215,26	239,24
PBIAS (mm/h)	8,54	2,30	-1,80	-4,30

It is noteworthy that the precipitations from the IMERG and TMPA products present high values for the MAE and RMSE indexes, indicating that the estimates were not very accurate. Regarding the PBIAS value, it can be seen that the values were negative, indicating a tendency of underestimation concerning the rain gauge stations values.

The results from the IMERG product corroborate with Teodoro et al. (2020), who, when assessing the accuracy of the IMERG product in a watershed in southeastern Brazil, observed underestimation tendencies regarding the data measured with rain gauge stations. It should be added that the underestimation of these results may be related to the short range of available data for the IMERG (2000–2013), as it showed the shortest range in this study.

It should be noted that the tendency of underestimating the results of the TMPA product is also reflected by its annual mean value and amplitude. Those values were, respectively, 8.2% and 53.3%, lower than the values from rain gauge stations. It must be noted that this behavior has already been observed by other authors, who highlighted the sudden change of the precipitation values in specific locations in the watersheds. Those locations are subject to tendencies of under or overestimation (CERA and FERRAZ, 2015). Thus, even if there is an indication of underestimation of the PPT_{TMPA}, in the general context, the behavior along the watershed varies.

The PPT_{IDW} presented high values for the MAE and RMSE indexes, which were similar to each other and indicated low accuracy of the estimates regarding the observed data, nevertheless, the errors were smaller than those recorded by PPT_{IMERG} and PPT_{TMPA}. With regard to the PBIAS index, the positive value, with a magnitude higher than the others, indicated a tendency to overestimate in relation to the observed values. The performance of PPT_{IDW} shows that the interference resulting from the interpolation with IDW method does not always lead to satisfactory results.

With regard to the PPT_{TC}, the values obtained for the MAE and RMSE indexes were the lowest among the variables (85.91 e 120.39, respectively), and showed that the PPT_{TC} was the most accurate variable. Regarding the PBIAS index, it is noted that the positive value (2.30) indicates that the estimated data tend to be greater than the measured ones.

In this regard, it is noteworthy that in addition to presenting the best statistical performance with reference to the data from rain gauge stations, PPT_{TC} was the variable that showed the greatest sensitivity to variations in the spatial distribution of precipitation, enabling the discretization of each region, such as the orographic effect in the west, the arid climate in the northeast of the watershed. In addition, the variation in the magnitude of values along the Paraguaçu river basin corresponds to what is described in the literature. Therefore, the PPT_{TC} variable was the one that led to the greatest representation of the precipitation behavior in the Paraguaçu river basin. Therefore, the PPT_{TC} variable was the one that led to the greatest representation of the precipitation behavior in the Paraguaçu river watershed.

3.3 Actual evapotranspiration

Figure 5 shows the actual evapotranspiration (ETR) maps from remote sensing products: MOD16 (2000–2013), GLEAM (1980–2013), MOD16rsp (2000–2013) and TerraClimate (1972–2013).

The identification of the ETR behavior is made easier by the spatial resolution of the remote sensing products. As can be seen in Fig. 5a, the MOD16 product, which has the best resolution among the analyzed images (1 km), presents a better discretization of the ETR behavior along the watershed. This behavior is well defined by the spatial distribution and it is highly sensitive to changes in magnitude, a fact evidenced by the sudden changes in ETR values in regions very close to each other.

To the images from the GLEAM product (Fig. 5b), the variation pattern of ETR values is not well defined, it is a trend that results from the spatial resolution (0.25º), and which hinders a better understanding of the ETR variation along the watershed. In addition to this difficulty, there are sudden fluctuations in the ETR magnitudes, however in neighboring cells. These aspects characterize the importance of spatial resolution for obtaining images with more defined behavior patterns and with a better understanding in the results analysis.

The $ETR_{MOD16rsp}$ map (Fig. 5c), generated from the compatibility of the spatial resolution of the MOD16 product with that of the GLEAM (0.25 °) product, shows a trend of variation of the values corresponding to the pattern of the behavior of the ETR_{MOD16}. In addition, it is important to notice that when the spatial resolution of the image originated from MOD16 changes, it causes discretization capacity loss attributed to the product, and makes $ETR_{MOD16rsp}$ as difficult to characterize as the ETR from the GLEAM product.

The ETR obtained with the TerraClimate product (Fig. 5d) makes it easy to identify the ETR spatial behavior, showing good definition in the characterization of the different magnitudes of the ETR and smoothing in the transition areas of the values along the watershed.

The actual evapotranspiration results from four different products are characterized by differences in the discretization of spatial behaviors and magnitude variations along the watershed (Fig. 5). Nevertheless, all products led to lower values of actual evapotranspiration in the northeast region of the watershed and to a gradual increase in the magnitude of the ETR towards the watershed's mouth.

The MOD16 product (ETR_{MOD16}) (Fig. 5a) presents a behavior characterized by marked variations of the ETR values in the middle portion of the watershed. The ETR is related to the altitude, conditions and characteristics of soil use, types of vegetation and weather conditions (RIBEIRO, 2020; COMPAORÉ et al. 2008), as well as with the way in which they were calculated. MOD16 performs a global classification of land use and occupation, in which 17 different classes are characterized (FRIEDL et al. 2002).

According to Ribeiro (2020), because it has pixels of 1 km², the images from MOD16 provide great detail, however, they can result in ETR estimate inconsistencies, as can be seen by the range of its amplitude variation ETR_{MOD16} (467 to 1,667 mm $year^{-1}$), highest among all products, and due to the high mean value of ETR_{MOD16} (792 mm $year^{-1}$). These inconsistencies can be attributed to errors related to the imprecise classification of land cover types and to the uncertainties associated with the input data, such as the fraction of photosynthetically active radiation, the leaf area index and the GMAO (Global Modeling and Assimilation Office) reanalysis meteorological data (MU et al. 2011).

On the actual evapotranspiration map from the GLEAM product (ETR_{GLEAM}) (Fig. 5b), magnitude variations are unlikely to happen and are irregularly distributed, mainly due to fluctuations in adjacent cells values. An explanation for this behavior is accredited to the way the ETR is calculated the by the GLEAM product, which differentiates only three sources of evaporation based on the type of terrestrial surface: bare soil, short vegetation and vegetation with high canopy (MIRALLES et al. 2011; MARTENS et

al. 2017). It is also observed the predominance of values in the range of 700 mm year^{-1}, which are distributed in the middle region of the watershed. It is also observed the decrease in the magnitude of values in the northeast region. The variation in the amplitude of the ETR_{GLEAM} is the littlest among the products (402 to 1,039 mm year^{-1}) and its annual average is 650 mm.

The ETR_{MOD16} and ETR_{GLEAM} spatial distributions follow the rainfall variation pattern, with high ETR magnitudes in regions where there are higher rainfall indexes and lower magnitudes in the regions where these indexes are lower. This trend was also listed by Moreira et al. (2019b) in the Brazilian Pantanal region, and by Moreira and Ruhoff (2019) in eight Brazilian watersheds, in which they analyzed the performance of the MOD16 and GLEAM product. They noted that for the Atlantic Eastern hydrographic region, where the Paraguaçu river watershed is inserted, both products tend to "follow" the occurrence of rain. It is noteworthy that this trend may be related to factors such as solar radiation, air temperature, wind speed, relative humidity and atmospheric pressure, characteristic of the semiarid climate.

On the $ETR_{MOD16rsp}$ map (Fig. 5c) the highest values are concentrated in the middle part of the watershed and close to its mouth, and the minimum values are distributed over a large area, covering the northeast region, a portion of the intermediate part and the far west region of the watershed. The average $ETR_{MOD16rsp}$ value (792 mm year^{-1}) is the same as the one obtained with ETR_{MOD16} (792 mm year^{-1}) however, the variation range of its values is smaller (572 to 1,242 mm year^{-1}).

The TerraClimate product (ETR_{TC}) (Fig. 5d) grants a better characterization of the variations in the ETR magnitude and spatial distribution when compared to the ETR_{GLEAM} and the $ETR_{MOD16rsp}$. Therefore, it makes it possible to record a sharp increase in values in the middle part of the watershed, a region that encompasses Chapada Diamantina, and a decrease of values as it approaches the northeast region of the watershed. It is also worth noting the gradual increase in values towards the watershed's mouth.

The ETR_{TC} behavior along the watershed is similar to the trend already mentioned before for ETR_{MOD16} and ETR_{GLEAM}, reaffirming the association with the precipitation. The performance of the products in detecting these variations is also noteworthy. In turn, TerraClimate uses climatologically aided interpolation, combining high spatial resolution climatological standards from the WorldClim data set, with more coarse spatial resolution from the Climate Research Unit (CRU Ts4.0) and the Japanese 55-year reanalysis (JRA55) (ABATZOGLOU et al. 2018). Finally, it seems that the ETR_{TC} amplitude varied from 402 to 1,089 mm year^{-1} and its average annual value (639 mm) was the lowest among the products.

In short, the MOD16 and TerraClimate products, which have the highest spatial resolutions, are also the ones with the highest amplitudes. The $ETR_{MOD16rsp}$, on the other hand, produces a variation range with an interval and magnitude lower than the ETR_{MOD16} origin variable, associated with the lower degree of detail of its spatial resolution. This behavior as well as the better ability of smaller pixels to represent the

different changes in land use, and thus directly throwback the ETR response (KHAN et al. 2018; RUHOFF et al. 2013).

In face of the evaluation of real evapotranspiration images in the Paraguaçu river basin, it is noted that the ETR maps are influenced by precipitation variations. However, among the information obtained by the products, the ETR_{TC} variable leads to the most consistent results in terms of spatial distribution and magnitude of values in each region, characterizing variations such as the orographic effect, influence of proximity to the coast and the semiarid climate. Therefore, considering its performance, the ETR_{TC} was the variable that best represented the actual evapotranspiration behavior in the watershed.

3.3 Water balance

In order to assess the water balance representativeness in the water circulation processes in the Paraguaçu River watershed, tests with the combination of precipitation and actual evapotranspiration images are obtained from different ways. Therefore, it is necessary to determine which combination has the best performance and whether the images with the best performance in the independent evaluation produce the best results, when combined.

Figure 6 shows the water balance maps considering the precipitation from the IMERG product, combined with four different sources of actual evapotranspiration (ETR_{MOD16}, $ETR_{MOD16rsp}$, ETR_{GLEAM} and ETR_{TC}).

The WB_{IMERG_MOD16} and $WB_{IMERG\_MOD16rsp}$ water balance maps, shown in Figs. 6 (a and b), present irregular behavior in terms of spatial distribution and magnitude of values (-709 to 99 mm $year^{-1}$ and −420 to 63 mm $year^{-1}$, respectively), in which the great extent of areas with marked negative values stands out (82.17% and 94.56%, respectively). This behavior can be justified by the tendency of the MOD16 product to have higher evapotranspiration values than precipitation (MIRALLES, 2016) due to the difficulty in consistently estimating evapotranspiration (RUHOFF et al. 2013).

The presence of negative values in water balance represents a limitation that can be attributed to the existence of inconsistencies in the product's input data, to the discretization provided by the spatial resolution and to the lower performance of the product in regions with orographic influence or in regions of semi-arid climate, in which have great precipitation variability and ETR high evaporative power.

The occurrence of a negative water balance is physically unlikely, given that, considering the constant water storage variation, this negative water balance results from the difference between the amount of water that comes from precipitation less the amount of water that leaves through evapotranspiration (SENTELHAS et al. 1999). Therefore, it is expected that the WB has a value greater than or equal to zero. The occurrence of negative values would imply the absence of water courses, characterizing the “disappearance” of the water without a physical justification. In the same way values close to or equal to zero would lead to intermittent rivers, since these values would not be enough to guarantee the maintenance/perpetuity of minimum flows, a scenario that also does not reflect the conditions of the negative areas in the watershed.

A determining factor for the existence of negative values in the water balance is the difficulty of estimating variables, such as evapotranspiration, which has a greater limitation for its establishment on large spatial scales (WANG et al. 2014).

In view the limitations inherent to the predominance of negative values in WB, suggest the analysis of other evapotranspiration databases in the estimation of water balance with remote sensing. In this sense, the use of these images (Figs. 6a and 6b) should be rejected, since they are not representative of the hydrological processes in the watershed and produce discrepancies that contradict the physical signs of the watershed.

In the water balances WB_{IMERG_GLEAM} and WB_{IMERG_TC} (Figs. 6c and 6d) the negative values (40% and 25%, respectively) are concentrated in the region where the orographic effect occurs and extends through the semiarid region (Fig. 2) in a less accentuated way than the previous WB ones. In general, the existence of the orographic effect produced a sharp increase in all ETR estimates values, due to the large altitude variations (HOUZE, 2011) and the climate transitions, from semi-arid to dry sub-humid climate. The ETR estimate influence in this process is emphasized, since the precipitation (PPT_{IMERG}) was not altered on the maps. The range of annual variation in the values of WB_{IMERG_GLEAM} and WB_{IMERG_TC} (-177 to 248 mm and − 138 to 257 mm, respectively) shows an increase in the magnitude of positive values and a reduction in the magnitude of negative values regarding the WB values already presented.

Figure 7 shows the water balance maps considering the precipitation from the TMPA product, combined with four different sources of actual evapotranspiration (ETR_{MOD16}, $ETR_{MOD16rsp}$, ETR_{GLEAM} and ETR_{TC}).

The water balances WB_{TMPA_MOD16} and $WB_{TMPA\_MOD16rsp}$ (Figs. 7a and 7b), have similar characteristics in terms of the spatial distribution of the values, with amplitudes (-482 to 63 mm $year^{-1}$ and − 338 to 60 mm $year^{-1}$, respectively), indicating the large percentage of areas with negative values (91% and 93%, respectively). It is observed that the use of the MOD16 ETR continues to produce major inconsistencies in the calculation of the water balance and generating high magnitudes in the negative values (see Figs. 7a and 7b). It is also noted that combinations of variables with unsatisfactory performances lead to poor results.

In Figs. 7c and 7d, WB_{TMPA_GLEAM} and WB_{TMPA_TC} present marked variations in the spatial distribution of values, whose amplitude (-152 to 210 mm $year^{-1}$ and − 73 to 208 mm $year^{-1}$, respectively) includes negative values that are located in the middle portion and in the northeast region of the watershed, and cover about 30% and 16% of the total area. Thus, the GLEAM product performs better for more humid regions, as it leads to a tendency for negative values to take place in regions with a semi-arid climate. The TerraClimate product, on the other hand, performs better in regions with lower rainfall, with a tendency for negative values to take place in regions with dry sub-humid climate (Fig. 7). It should be noted that both perform better than the MOD16 product along the watershed.

Figure 8 shows the water balance maps considering the precipitation data of rain gauge stations, interpolated with IDW, combined with four different sources of actual evapotranspiration (ETR_{MOD16}, $ETR_{MOD16rsp}$, ETR_{GLEAM} and ETR_{TC}).

The WB_{IDW_MOD16} and $WB_{IDW\_MOD16rsp}$ (Figs. 8a and 8b) water balances show spatial variations close to each other, mostly composed of negative values (about 58% and 70% of the total area). In this case, these inconsistencies may be associated with the shortage of rain gauge stations to detect the spatial variability of the precipitation and support the level of detail presented on the map (RIBEIRO, 2020). The variation range of WB_{IDW_MOD16} is the largest among all maps (-772 to 855 mm $year^{-1}$) and $WB_{IDW\_MOD16rsp}$ has the lowest annual range, ranging from – 394 to 533 mm.

Regarding the WB_{IDW_GLEAM} (Fig. 8c), it is observed that the variation of values trend in the watershed (-242 to 731 mm $year^{-1}$) corresponds to the behavior of PPT_{IDW} precipitation, especially when estimating high values in the northeast portion of the watershed and to generate areas with negative values (24.88%) in regions with less rainfall, such as the central part of the watershed.

The failure to balance the inputs and outputs of the WB is evidence that reinforces the existence of inaccuracies in the generated estimates, with the use of remote sensing tools. This procedure has an obstacle, when it comes to comparing data with estimates made with models (MOREIRA, 2018). Therefore, the performance evaluation of a product or remote sensing methodology must be carried out together with the behavior analysis of the hydrological processes in the study area, in order to guarantee the representativeness of the results.

WB_{IDW_TC} (Fig. 8d) leads to a spatial distribution similar to the one presented with WB_{IDW_GLEAM}, but with a smaller percentage of negative areas (10.49%) and lesser variation of values range (-166 to 661 mm $year^{-1}$). It is noted that the occurrence of negative values is also associated with the precipitation variability and the evapotranspiration interannual variability, since these are strongly related. In semiarid regions, the potential evapotranspiration balance is more or less considered depending on the amount of rainfall during the year (FELIX and PAZ, 2016).

Figure 9 Water balance obtained with the TerraClimate precipitation and the ETR_{MOD16} (a), $ETR_{MOD16rsp}$ (b), ETR_{GLEAM} (c) and ETR_{TC} (d) for the Paraguaçu river watershed. WBmax corresponds to the maximum value of WB for each source and WBmin corresponds to the minimum value of WB for each source

In the WB_{TC_MOD16} and $WB_{TC\_MOD16rsp}$ water balances (Figs. 9a and 9b) the spatial distribution is characterized, predominantly, by areas with negative values (70% and 82%, respectively). The amplitude variation range of WB_{TC_MOD16} (-700 to 673 mm $year^{-1}$) corresponds to twice the range of variation of $WB_{TC\_MOD16rsp}$ (-374 to 292 mm $year^{-1}$). According to the study developed by Ribeiro (2020), the use of the MOD16 product in the Jequitinhonha watershed, in the Brazilian semiarid region, also generated negative values in the water balance, due to inconsistencies attributed to the product for regions with low

precipitation. It is noteworthy that for the Paraguaçu river watershed the same behavior is observed, where the MOD16 product produced negative values with greater extension and magnitude in all combinations.

In the WB_{TC_GLEAM} water balance (Fig. 9c), the existence of negative values (22.35% of the area) follows the precipitation trend, and is displayed in the regions where it has the lowest magnitude. Regarding the annual amplitude (-179 to 428 mm), WB_{TC_GLEAM} presents positive values that are more representative than the WB generated with MOD16. Performance that may be associated with the way the ETR was calculated with GLEAM (Priestley-Taylor Equation), with a small number of inputs, mainly considering the use of data sets based on satellite observations, from diverse and well validated sources, minimizing the use of data modelling and parameterizations (MOREIRA et al. 2019a).

Lastly, WB_{TC_TC} (Fig. 9d) presents variations characterized by greater magnitudes in the western region and smoothed behavior in the eastern region of the watershed, corresponding to the pluviometric regime and representing variations in the climate types in the watershed (Fig. 2). The WB_{TC_TC} configuration was the only one that did not produce areas with negative values, producing a range of variation (22 to 431 mm $year^{-1}$) with consistent behavior and reaffirming its best performance regarding the other products. An explanation for this performance is due to the fact that both components (PPT and ETR) come from the same database (TerraClimate), have the same data range and have presented the best performances in the individualized analysis.

The use of the water balance to evaluate the estimates of its components adds valuable information about the behavior of the hydrological cycle in the watershed. Among the different combinations of WB, the performance of the WB_{TC_TC} and WB_{IDW_TC} variables were superior. WB_{IDW_TC} presented the lowest percentage of areas with negative values and spatial variations that follow the behavior of PPT_{IDW}. The WB_{TC_TC} on the other hand, did not record negative WB values, it was generated by the combination of images, from the TerraClimate product, which presented better performance in the individualized analysis. In addition, the variations along the watershed corroborate with the pattern found in other publications, regarding the characteristics of climate, relief and amplitude range of the values variation. Therefore, the WB_{TC_TC} variable is the one that best represents the conditions of water circulation in the watershed of the Paraguaçu river.

4. Conclusions

The consideration of variables that provide reliable estimates and consistent with the study site is very important, as these conditions are essential for the advancement of planning and management of water resources. In this sense, the present work approaches the evaluation of the water balance generated with the combination of precipitation and real evapotranspiration from different databases, in order to obtain the best representation of the hydrological processes in the hydrographic basin.

Precipitation from the TerraClimate database (PPT_{TC}) led to a better discretization of spatial behavior in the watershed, characterizing variations in orography, greater humidity in regions close to the coast and aridity indices of the semiarid climate. In addition, the PPT_{TC} variable presented the best statistical performance, and, therefore, generated the most representative results.

The actual evapotranspiration obtained by the TerraClimate database (ETR_{TC}) presented results with magnitudes lower than the precipitations and with good spatial distribution in each region of the watershed, characterizing the different biomes and varying according to the types of climates, such as the orographic effect and the semiarid.

The combination of the PPT_{TC} and ETR_{TC} variables, with the best performance in the individualized analysis, led to the water balance (WB_{TC_TC}) more representative of the water circulation conditions in the watershed. It was the only variable that did not produce negative values and that presented a behavior consistent with the hydrological processes.

Declarations

Funding

This study was financed in part by the Coordenação de Aperfeiçoamento de Pessoal de Nível Superior - Brasil (CAPES) - Finance Code 001.

Conflicts of interest/Competing interests

The authors declare that they have no known competing financial interests or personal relationships that could have appeared to influence the work reported in this paper.

Ethics approval/declarations

Not applicable, because this article does not contain any studies with human or animal subjects..

Consent to Participate

The authors declare that they participated in the preparation of the manuscript.

Consent for publication

The authors declare that they agree with the publication of the manuscript.

Availability of data and material/ Data availability

All data generated or analysed during this study are included in this published article [and its supplementary information files].

Code Availability

This work did not produce any software application or custom code to be made available.

Authors' Contributions

AKN: Conceptualization, Methodology, Writing—Original Draft, Writing—Review & Editing; FFP: Conceptualization, Methodology, Writing— Original Draft, Writing—Review & Editing; RBR: Methodology, Writing—Review & Editing, Visualization. All authors read and approved the final manuscript.

References

1. ABATZOGLOU JT, DOBROWSKI SZ, PARKS SA, HEGEWISCH KC (2018) TerraClimate, a high-resolution global dataset of monthly climate and climatic water balance from 1958–2015. **Scientific data**, v. 5, n. 1, p. 1–12, https://doi.org/10.1038/sdata.2017.191
2. ALLEN RG, PEREIRA LS, HOWELL TA, JENSEN ME (2011) Evapotranspiration information reporting: II recommended documentation. **Agricultural Water Management**, v. 98, n. 6. 921–929. https://doi.org/10.1016/j.agwat.2010.12.016
3. ALVARES CA, STAPE JL, SENTELHAS PC, GONÇALVES JLM, SPAROVEK G (2013) Köppen's climate classification map for Brazil. Meteorologische Zeitschrift, v. 22, n. 6. 711–728. https://doi.org/10.1127/0941-2948/2013/0507
4. CARELLI L, SANTO SM Semeando águas no Paraguaçu / organizadores: Ivana R. Lamas, S471 Luciana Santa Rita, Rogério Mucugê Miranda. – Rio de Janeiro
5. Conservação Internacional (2016) Brasil,
6. CERA JC, FERRAZ SET (2015) Variações climáticas na precipitação no sul do Brasil no clima presente e futuro. **Revista Brasileira de Meteorologia**, v. 30, n. 1. 81–88. https://doi.org/10.1590/0102-778620130588
7. COMPAORÉ H, HENDRICKX JM, HONG SH, FRIESEN J, VAN DE GIESEN NC, RODGERS C, VLEK PL (2008) Evaporation mapping at two scales using optical imagery in the White Volta Basin, Upper East Ghana. **Physics and Chemistry of the Earth**, Parts A/B/C, v. 33, n. 1–2, p. 127–140, https://doi.org/10.1016/j.pce.2007.04.021
8. EDUARDO EN, MELLO CRD, VIOLA MR, OWENS PR (2016) CURI, N. Hydrological simulation as subside for management of surface water resources at the Mortes River Basin. **Ciência e Agrotecnologia**, v. 40, n. 4. 390–404. https://doi.org/10.1590/1413-70542016404009516
9. DINKU T, CECCATO P, CONNOR SJ (2011) Challenges of satellite rainfall estimation over mountainous and arid parts of east Africa. **International Journal of Remote Sensing**, v. 32, n. 21. 5965–5979. https://doi.org/10.1080/01431161.2010.499381
10. FELIX V, de PAZ S (2016) da. Representação dos processos hidrológicos em bacia hidrográfica do semiárido paraibano com modelagem hidrológica distribuída. **RBRH**, v. 21, n. 3. 556–569. https://doi.org/10.1590/2318-0331.011616009

11. FILL HD, SANTOS I, FERNANDES C, TOCZECK A, de OLIVEIRA MF (2005) Balanço hídrico da bacia do Rio Barigui, PR. **Raega - O Espaço Geográfico em Análise**. http://dx.doi.org/10.5380/raega.v9i0.3447. 9
12. FISHER JB, MELTON F, MIDDLETON E, HAIN C, ANDERSON M, ALLEN R KILIC, A. The future of evapotranspiration:Global requirements for ecosystem functioning, carbon and climate feedbacks, agricultural management, and water resources.Water Resources Research, v. 53, n.4 p. 2618-2626, 2017. https://doi.org/10.1002/2016wr020175
13. FLERCHINGER, G. N.; HANSON, C. L.; WIGHT, J. R. Modeling evapotranspiration and surface energy budgets across a watershed. **Water Resources Research**, v.32, p.2539-2548, 1996. https://doi.org/10.1029/96WR01240
14. FOX, D. G. Judging air quality model performance. Bulletin of the American Meteorological Society. American Meteorological Society. [s.l.], v. 62, n. 5, p.599-609, 1981. https://doi.org/10.1175/1520-0477(1981)062<0599:jaqmp>2.0.co;2
15. FRIEDL, M. A. Relationships among remotely sensed data, surface energy balance, and area-averaged fluxes over partially vegetated land surfaces. **Journal of Applied Meteorology**, v. 35, n. 11, p. 2091-2103, 1996. https://doi.org/10.1175/1520-0450(1996)035<2091:rarsds>2.0.co;2
16. FRIEDL MA, MCIVER DK, HODGES JCF, ZHANG XY, MUCHONEY D, STRAHLER AH, WOODCOCK CE, GOPAL S, SCHNEIDER A, COOPER A, BACCINI A, GAO F, SCHAAF C (2002) Global land cover mapping from MODIS: algorithms and early results. **Remote Sensing of Environment**, v. 83, n. 1–2. 287–302. https://doi.org/10.1016/s0034-4257(02)00078-0
17. GAO H, TANG Q, FERGUSON CR, WOOD EF, LETTENMAIER DP (2010) Estimating the water budget of major US river basins via remote sensing. Int J Remote Sensing 31:3955–3978. https://doi.org/10.1080/01431161.2010.483488
18. GENZ F, SILVA SF, TANAJURA CAS (2012) Impacto das mudanças climáticas nas vazões do rio Paraguaçu – Cenário A1B de 2011 a 2040. IN: **XI Simpósio de Recursos Hídricos do Nordeste. Anais**. João Pessoa – PB
19. GUPTA HV, SOROOSHIAN S, YAPO PO (1999) Status of automatic calibration for hydrologic models: Comparison with multilevel expert calibration. **Journal of hydrologic engineering**, v. 4, n. 2, p. 135–143, https://doi.org/10.1061/(asce)1084-0699(1999)4:2(135)
20. HAYASHI M, VAN DER KAMP G, ROSENBERRY DO (2016) Hydrology of prairie wetlands: understanding the integrated surface-water and groundwater processes. **Wetlands**, v. 36, n. 2, p. 237–254, https://doi.org/10.1007/s13157-016-0797-9
21. HOU AY, KAKAR RK, NEECK S, AZARBARZIN AA, KUMMEROW CD, KOJIMA M, IGUCHI T (2014) The global precipitation measurement mission. **Bulletin of the American Meteorological Society**, v. 95, n. 5. 701–722. https://doi.org/10.1175/bams-d-13-00164.1
22. HOUZE RA Jr (2012) Orographic effects on precipitating clouds. **Reviews of Geophysics**, v. 50, n. https://doi.org/10.1029/2011RG000365. 1

23. KHAN MS, LIAQAT UW, BAIK J, CHOI M (2018) Stand-alone uncertainty characterization of GLEAM, GLDAS and MOD16 evapotranspiration products using an extended triple collocation approach. **Agricultural and Forest Meteorology**, v. 252. 256–268. https://doi.org/10.1016/j.agrformet.2018.01.022
24. LELIS LCS, BOSQUILIA RW, DUARTE SN (2018) Avaliação dos dados de precipitação gerados pelos satélites GPM e TRMM. **Revista Brasileira de Meteorologia**, v. 33, n. 1. 153–163. https://doi.org/10.1590/0102-7786331004
25. LETTENMAIER DP, ALSDORF D, DOZIER J, HUFFMAN GJ, PAN M, WOOD EF (2015) Inroads of remote sensing into hydrologic science during the WRR era. **Water Resources Research**, v. 51, n. 9. 7309–7342. https://doi.org/10.1002/2015wr017616
26. LI Z, LIU WZ, ZHANG XC, ZHENG FL (2009) Impacts of land use change and climate variability on hydrology in an agricultural catchment on the Loess Plateau of China. **Journal of Hydrology**, v. 377, n. 1–2. 35–42. https://doi.org/10.1016/j.jhydrol.2009.08.007
27. LIAQAT UW, CHOI M (2017) Accuracy comparison of remotely sensed evapotranspiration products and their associated water stress footprints under different land cover types in korean peninsula. **Journal of Cleaner Production**, Elsevier, v. 155. 93–104. https://doi.org/10.1016/j.jclepro.2016.09.022
28. LONG D, LONGUEVERGNE L, SCANLON BR (2014) Uncertainty in evapotranspiration from land surface modeling, remote sensing, and GRACE satellites. Water Resour Res 50:1131–1151. https://doi.org/10.1002/2013wr014581
29. MARTENS B, MIRALLES DG, LIEVENS H, SCHALIE RVD, JEU RA (2017) VERHOEST, N. Gleam v3: Satellite-based land evaporation and root-zone soil moisture. **Geoscientific Model Development**, Copernicus GmbH, v. 10, n. 5. 1903–1925. https://doi.org/10.5194/gmd-2016-162. PRIETOD. F.BECK, H. E.; DORIGO, W.
30. MCCABE MF, RODELL M, ALSDORF DE, MIRALLES DG, UIJLENHOET R, WAGNER W, WOOD EF (2017) The future of Earth observation in hydrology. **Hydrology and earth system sciences**, v. 21, n. 7. 3879–3914. https://doi.org/10.5194/hess-21-3879-2017
31. MEDEIROS Y (2003) Análise dos Impactos das Mudanças Climáticas em Região Semiárida. **Revista Brasileira de Recursos Hídricos**, v. 8, n. 2, p. 127–136, https://doi.org/10.21168/rbrh.v8n2.p127-136
32. MIRALLES DG, HOLMES TRH, DE JEU RAM, GASH JH, MEESTERS AGCA, DOLMAN AJ (2011) Global land-surface evaporation estimated from satellite-based observations. **Hydrology and Earth System Sciences**, v. 15, n. 2. 453–469. https://doi.org/10.5194/hess-15-453-2011
33. MOHEBZADEH H, FALLAH M (2019) Quantitative analysis of water balance components in Lake Urmia, Iran using remote sensing technology. **Remote Sensing Applications**: **Society and Environment**, v. 13, p. 389–400, https://doi.org/10.1016/j.rsase.2018.12.009
34. MOREIRA AA, RUHOFF AL, ROBERTI DR, SOUZA V, de ROCHA A, PAIVA HR (2019) a R. C. Assessment of terrestrial water balance using remote sensing data in South America. **Journal of Hydrology**, v. 575, p. 131–147, https://doi.org/10.1016/j.jhydrol.2019.05.021

35. MOREIRA AA, FASSONI-ANDRADE AC, RUHOFF AL, PAIVA RC (2019b) Water balance based on remote sensing data in pantanal. **R. Ra'e Ga**, v. 46, n. 3. 20–32. http://dx.doi.org/10.5380/raega.v46i3.67096
36. MOREIRA AA, RUHOFF AL Evapotranspiração em bacias hidrográficas no Brasil: padrões e fatores limitantes. **Simpósio Brasileiro de Sensoriamento Remoto (19.: 2019 abr.: Santos, SP). Anais.** São José dos Campos: INPE, 2019
37. MU Q, ZHAO M, RUNNING SW (2011) Improvements to a modis global terrestrial evapotranspiration algorithm. **Remote Sensing of Environment**, Elsevier, v. 115, n. 8, p. 1781–1800, https://doi.org/10.1016/j.rse.2011.02.019
38. MU Q, HEINSCH FA, ZHAO M, RUNNING SW (2007) Development of a global evapotranspiration algorithm based on MODIS and global meteorology data. **Remote Sensing of Environment**, v. 111, n. 4. 519–536. https://doi.org/10.1016/j.rse.2007.04.015
39. NANDI S, MANNE JR (2020) Spatiotemporal Analysis of Water Balance Components and Their Projected Changes in Near-future Under Climate Change Over Sina Basin, India. **Water Resources Management**, v. 34. 2657–2675. https://doi.org/10.1007/s11269-020-02551-2
40. RAMOELO A, MAJOZI N, MATHIEU R, JOVANOVIC N, NICKLESS A, DZIKITI S (2014) Validation of global evapotranspiration product (MOD16) using Flux tower data in the African Savanna, South Africa. **Remote Sensing**, v. 6, n. 8. 7406–7423. https://doi.org/10.3390/rs6087406
41. RIBEIRO RB (2020) **Aprimoramento do processo de estimativa da disponibilidade hídrica**/ Tese de Doutorado – Engenharia Agrícola. Universidade Federal de Viçosa, Viçosa, MG
42. ROUHOLAHNEJAD FREUND E, FAN Y, KIRCHNER JW (2020) Global assessment of how averaging over spatial heterogeneity in precipitation and potential evapotranspiration affects modeled evapotranspiration rates. **Hydrology and Earth System Sciences**, v. 24, n. 4. 1927–1938. https://doi.org/10.5194/hess-24-1927-2020
43. RUHOFF AL, PAZ AR, ARAGAO LEOC, MU Q, MALHI Y, COLLISCHONN W, ROCHA HR, RUNNING SW (2013) Assessment of the MODIS global evapotranspiration algorithm using eddy covariance measurements and hydrological modelling in the Rio Grande basin. **Hydrological Sciences Journal**, v. 58, n.8. 1658–1676. https://doi.org/10.1080/02626667.2013.837578
44. SENTELHAS PC, PEREIRA AR, MARIN R, ANGELOCCI LR, ALFONSI RR, CARAMORI PH, SWART S (1999) Balanço hídrico climatológico no Brasil. [CD ROM]. Esalq/USP–Piracicaba
45. SERRÃO EADO, WANZELER RTS, SANTOS CAD, GONÇALVES LDJM, LIMA AMMD, ROCHA E (2016) J. P. D. Avaliação estatística entre as estimativas de precipitação da constelação GPM com TRMM: Uma análise a bacia hidrográfica do rio Solimões. **Revista brasileira de climatologia**, v. 18, http://dx.doi.org/10.5380/abclima.v18i0.43059
46. SHEFFIELD J, FERGUSON CR, TROY TJ, WOOD EF, MCCABE MF (2009) Closing the terrestrial water budget from satellite remote sensing, **Geophysical Research Letters**, v. 36, n. https://doi.org/10.1029/2009gl037338. 7

47. SIRISENA TA, MASKEY, Shreedhar (2020) RANASINGHE, Roshanka. Hydrological Model Calibration with Streamflow and Remote Sensing Based Evapotranspiration Data in a Data Poor Basin. **Remote Sensing**, v. 12, n. 22. 3768. https://doi.org/10.3390/rs12223768
48. SKOFRONICK-JACKSON G, PETERSEN WA, BERG W, KIDD C, STOCKER EF, KIRSCHBAUM DB, WILHEIT T (2017) The Global Precipitation Measurement (GPM) mission for science and society. **Bulletin of the American Meteorological Society**, v. 98, n. 8. 1679–1695. https://doi.org/10.1175/BAMS-D-15-00306.1
49. SOUSA F, MACEDO MJH, GUEDES RDS, SILVA V (2016) O Índice de Precipitação Padronizada (IPP) na identificação de extremos de chuvas e secas na bacia do rio Paraguaçu (BA). **Ambiência**, v. 12, n. 2, p. 707–719, https://doi.org/10.5935/ambiencia.2016.02.14
50. TANAJURA CAS, GENZ F, de ARAÚJO HA (2010) Mudanças climáticas e recursos hídricos na Bahia: validação da simulação do clima presente do HadRM3P e comparação com os cenários A2 e B2 para 2070–2100. **Revista Brasileira de Meteorologia**, v. 25, n. 3. 345–358. https://doi.org/10.1590/S0102-77862010000300006
51. TEODORO TA, PASSOS RB, SILVA BA, SILVA BC (2020) da. Análise das Estimativas da precipitação diária do produto GPM-IMERG na bacia hidrográfica do rio Sapucaí, região sudeste do Brasil. **Anuário do Instituto de Geociencias**, v. 43, n. 2, https://doi.org/10.11137/2020_2_449_459
52. VALÉRIO E, de FRAGOSO LS, JUNIOR CR (2015) Avaliação dos efeitos de mudanças climáticas no regime hidrológico da bacia do rio Paraguaçu, BA. **Revista Brasileira de Recursos Hídricos**, v. 20, n. 4, p. 872–887, https://doi.org/10.21168/rbrh.v20n4.p872-887
53. WANG X, HUANG G, LIN Q, NIE X, CHENG G, FAN Y, LI Z, YAO Y, SUO (2013) M. A stepwise cluster analysis approach for downscaled climate projection – A Canadian case study. Environmental Modelling & Software, v. 49, p. 141–151, https://doi.org/10.1016/j.envsoft.2013.08.006
54. YANG S, NESBITT SW (2014) Statistical properties of precipitation as observed by the TRMM precipitation radar. **Geophysical Research Letters**, v. 41. 5636–5643. https://doi.org/10.1002/2014gl060683
55. ZHANG Y, PAN M, SHEFFIELD J, SIEMANN AL, FISHER CK, LIANG M, WOOD EF (2018) A Climate Data Record (CDR) for the global terrestrial water budget: 1984–2010. **Hydrology and Earth System Sciences**, v. 22, n. 1. 241–263. https://doi.org/10.5194/hess-22-241-2018
56. ZHOU Y, LAU WKM, HUFFMAN GJ (2015) Mapping TRMM TMPA into average recurrence interval for monitoring extreme precipitation events. **Journal of Applied Meteorology and Climatology**, v. 54. 979–995. https://doi.org/10.1175/JAMC-D-14-0269.1
57. WANG, X.; HUANG, G.; LIN, Q.; NIE, X.; CHENG, G.; FAN, Y.; LI, Z.; YAO, Y.; SUO, M. A stepwise cluster analysis approach for downscaled climate projection – A Canadian case study. **Environmental Modelling & Software**, v. 49, p. 141–151, 2013. https://doi.org/10.1016/j.envsoft.2013.08.006
58. YANG, S.; NESBITT, S. W. Statistical properties of precipitation as observed by the TRMM precipitation radar. **Geophysical Research Letters**, v. 41, p. 5636–5643, 2014. https://doi.org/10.1002/2014gl060683

59. ZHANG, Y.; PAN, M.; SHEFFIELD, J.; SIEMANN, A. L.; FISHER, C. K.; LIANG, M.; WOOD, E. F. A Climate Data Record (CDR) for the global terrestrial water budget: 1984–2010. **Hydrology and Earth System Sciences**, v. 22, n. 1, p. 241–263, 2018. https://doi.org/10.5194/hess-22-241-2018

60. ZHOU, Y.; LAU, W. K. M.; HUFFMAN, G. J. Mapping TRMM TMPA into average recurrence interval for monitoring extreme precipitation events. **Journal of Applied Meteorology and Climatology**, v. 54, p. 979–995, 2015. https://doi.org/10.1175/JAMC-D-14-0269.1

Figures

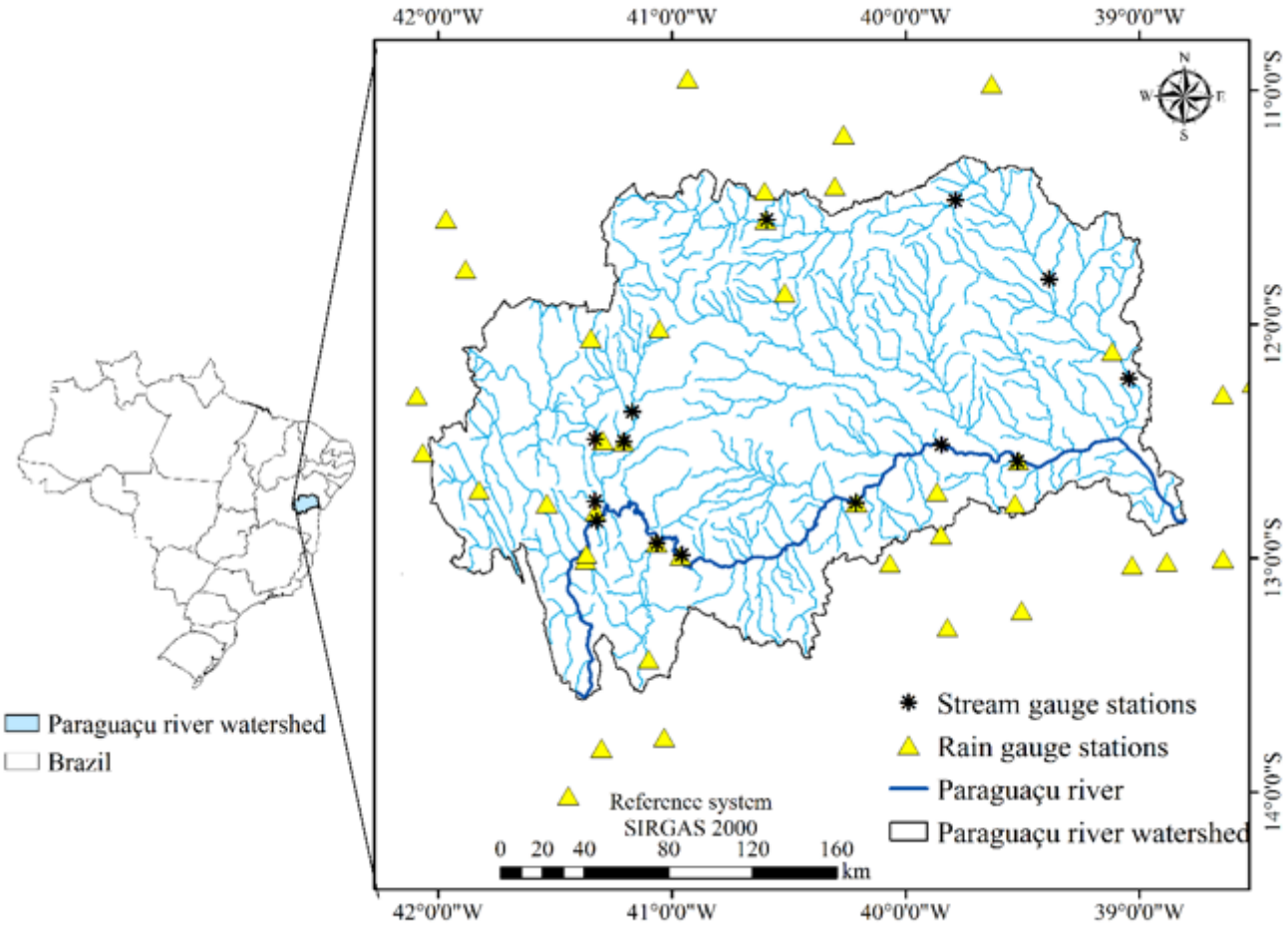

Figure 1

Location of the Paraguaçu river watershed in relation to the Brazil and selected stream gauge and rain gauging stations

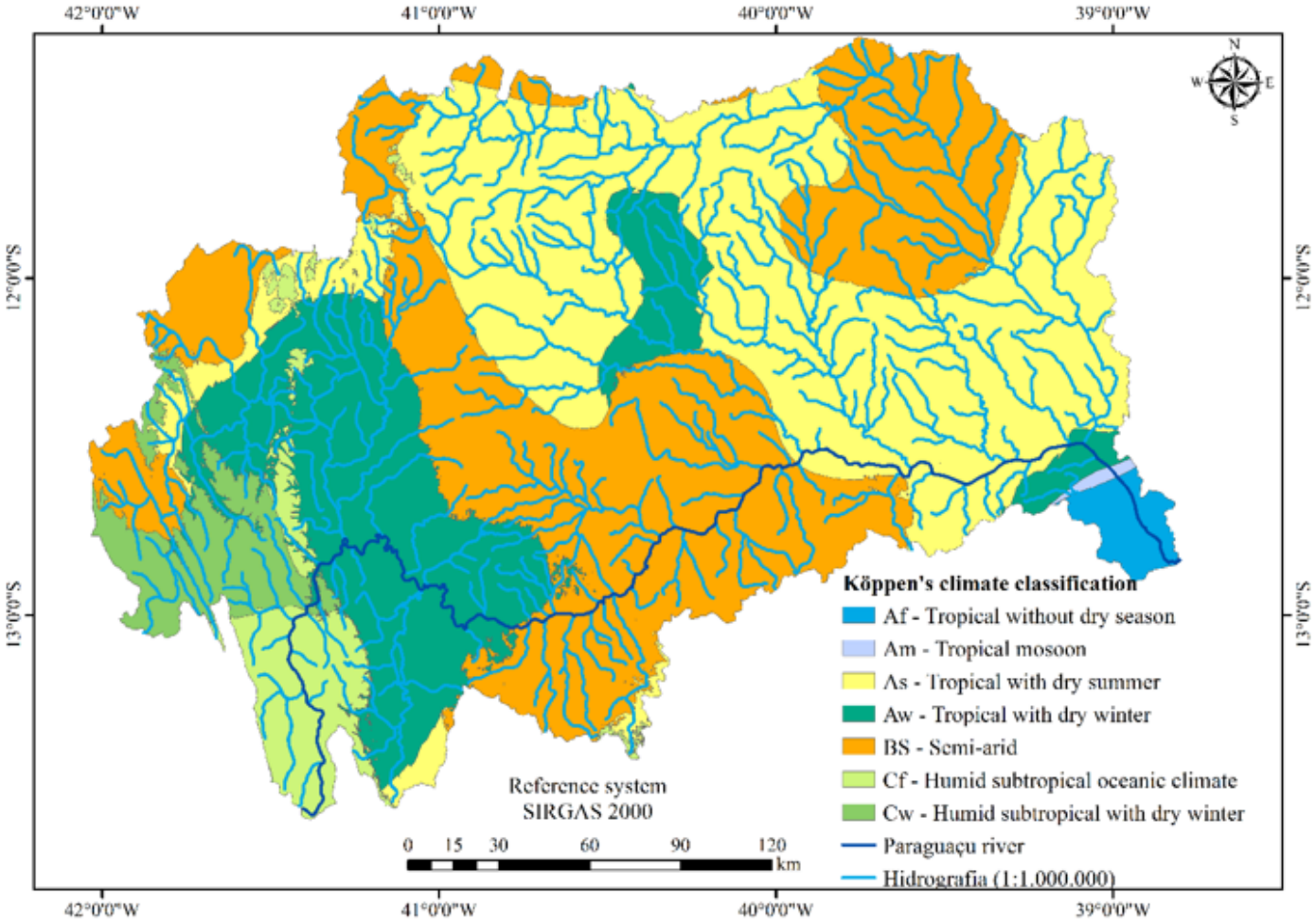

Figure 2

Climate types in the Paraguaçu River watershed. Source: Adapted from Alvares et al. (2013)

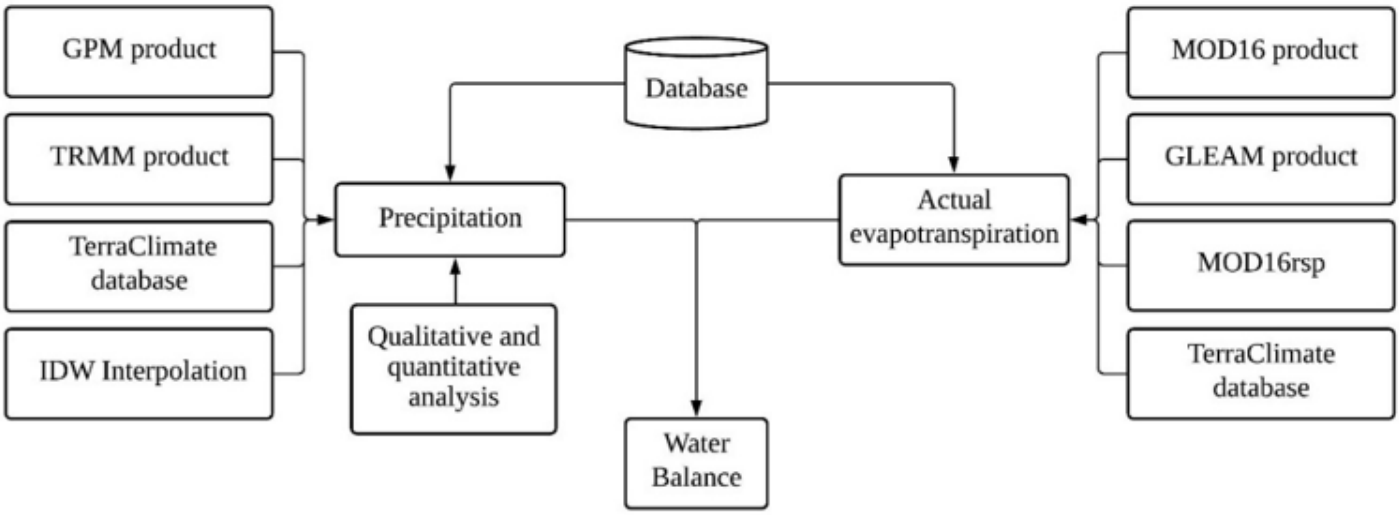

Figure 3

Flowchart with the steps of this study

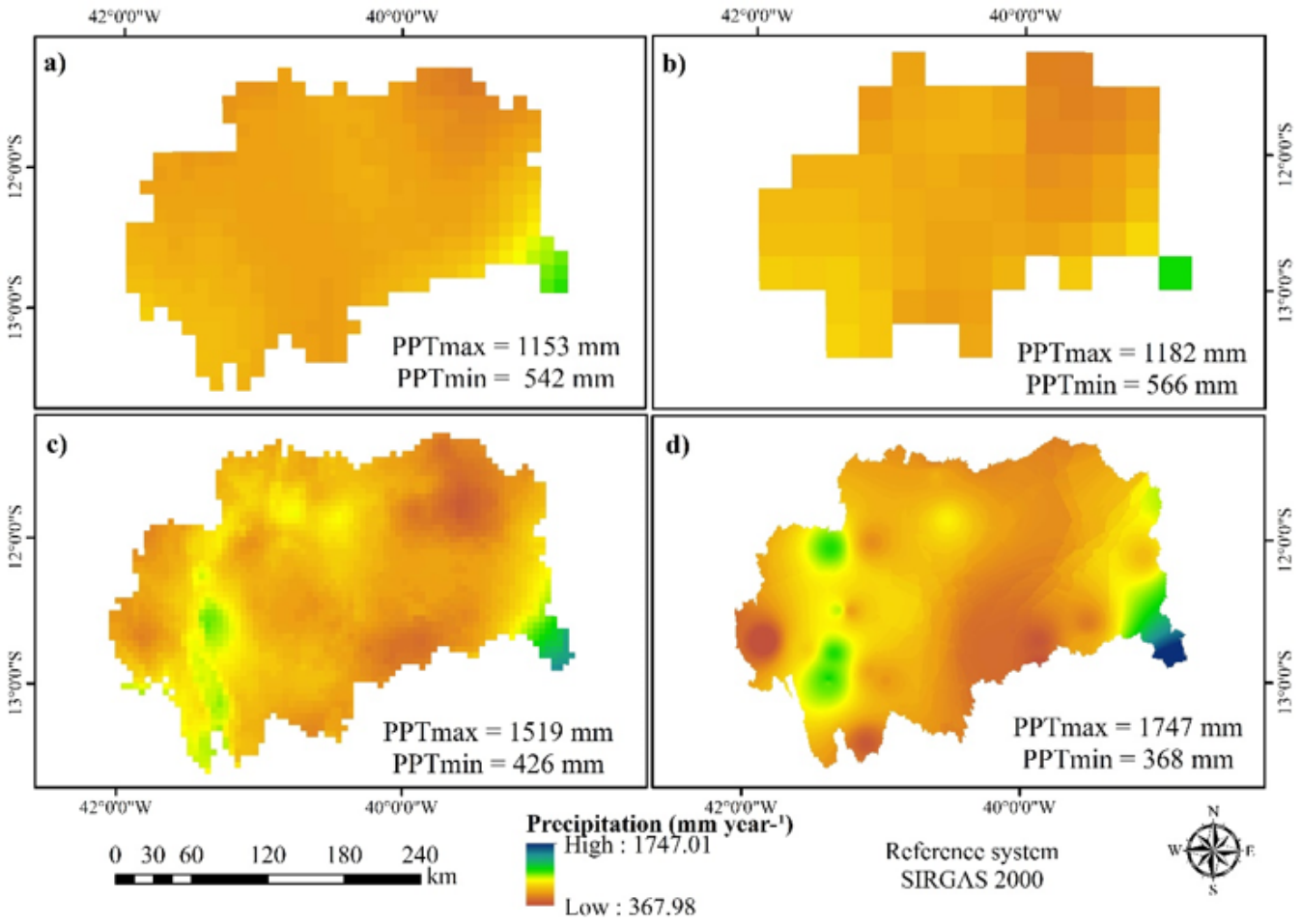

Figure 4

Precipitation maps obtained with the remote sensing products IMERG (a), TMPA (b), TerraClimate (c) and interpolated with IDW (d) for the Paraguaçu river watershed. PPTmax corresponds to the maximum value of PPT for each source and PPTmin corresponds to the minimum value of PPT for each source

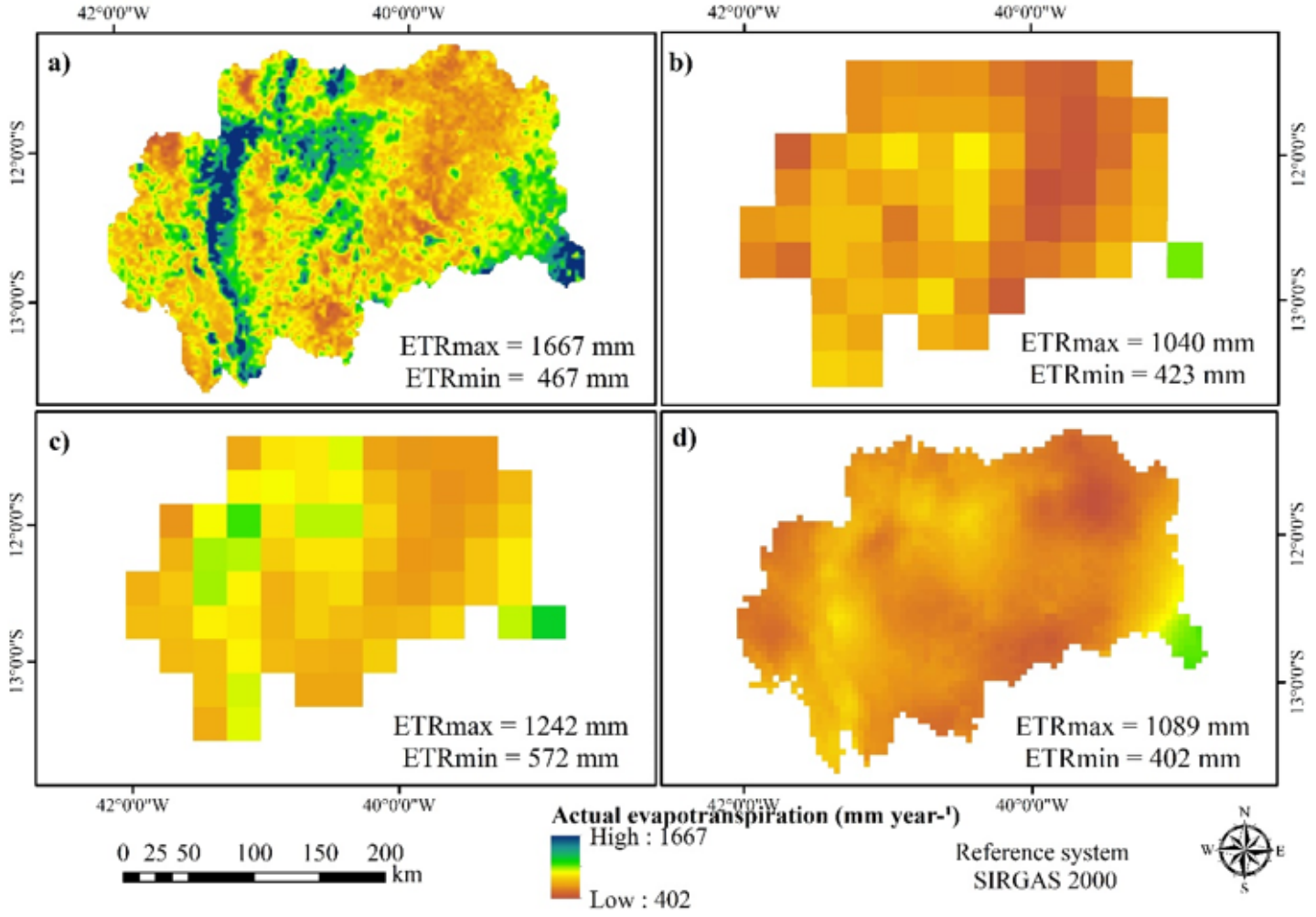

Figure 5

Actual evapotranspiration maps obtained with MOD16 (a), GLEAM (b), MOD16rsp (c) and TerraClimate (d) products for the Paraguaçu river watershed. ETRmax corresponds to the maximum value of ETR for each source and ETRmin corresponds to the minimum value of ETR for each source

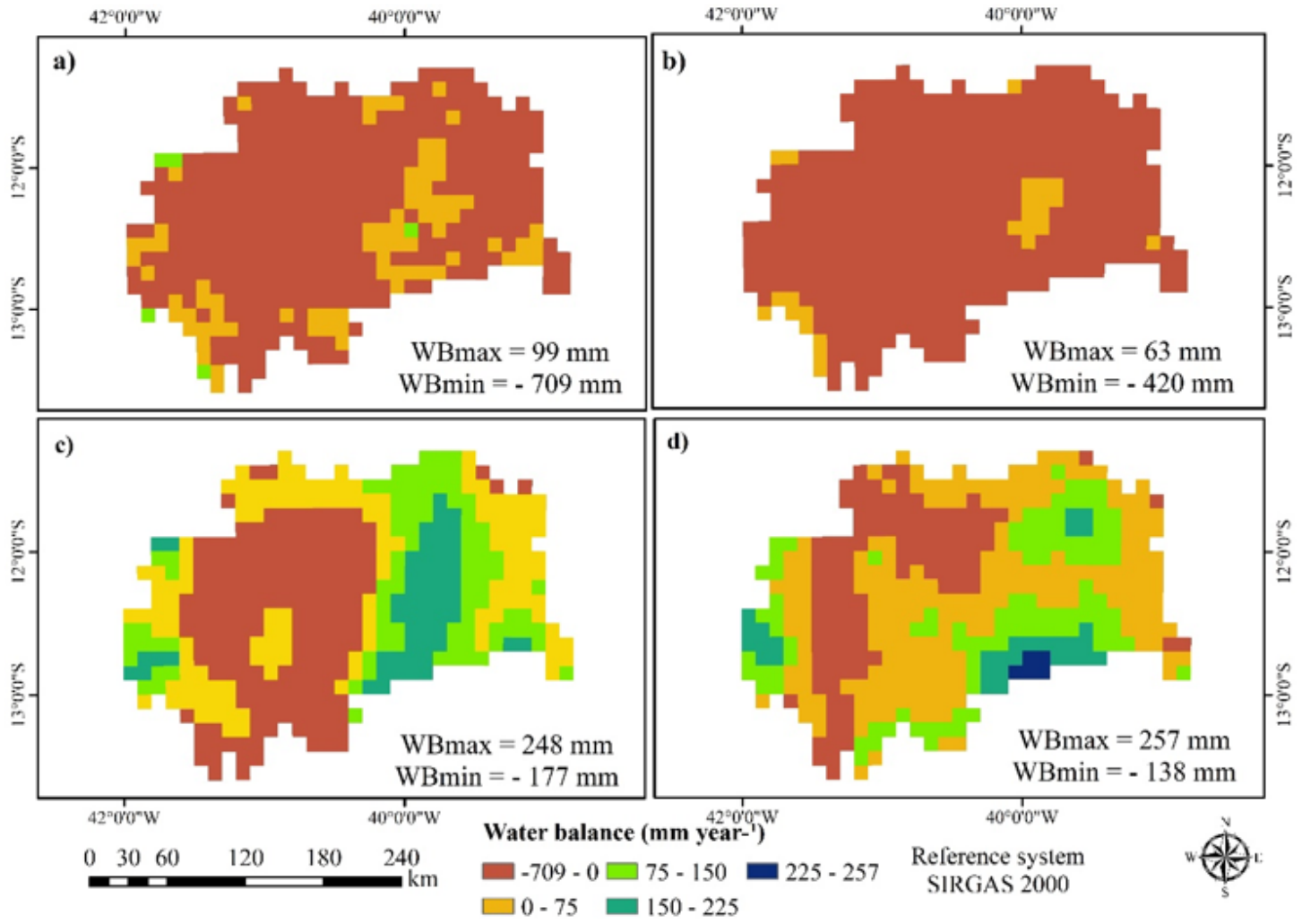

Figure 6

Water balance obtained by combining IMERG precipitation and ETR_{MOD16} (a), $ETR_{MOD16rsp}$ (b), ETR_{GLEAM} (c) and ETR_{TC} (d) for the Paraguaçu river watershed. WBmax corresponds to the maximum value of WB for each source and WBmin corresponds to the minimum value of WB for each source

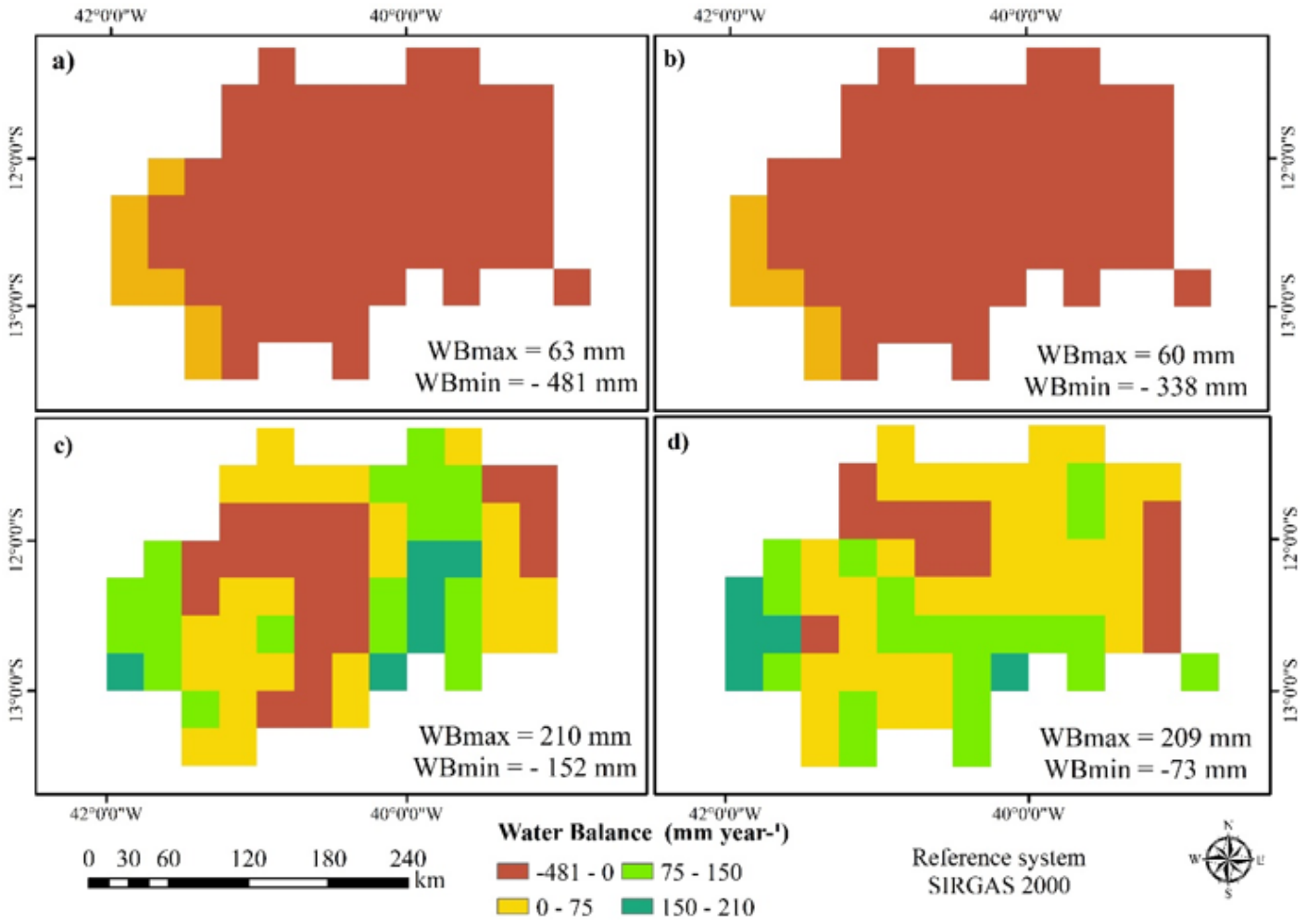

Figure 7

Water balance obtained with the TMPA precipitation and the ETR_{MOD16} (a), $ETR_{MOD16rsp}$ (b), ETR_{GLEAM} (c) and ETR_{TC} (d) for the Paraguaçu river watershed. WBmax corresponds to the maximum value of WB for each source and WBmin corresponds to the minimum value of WB for each source

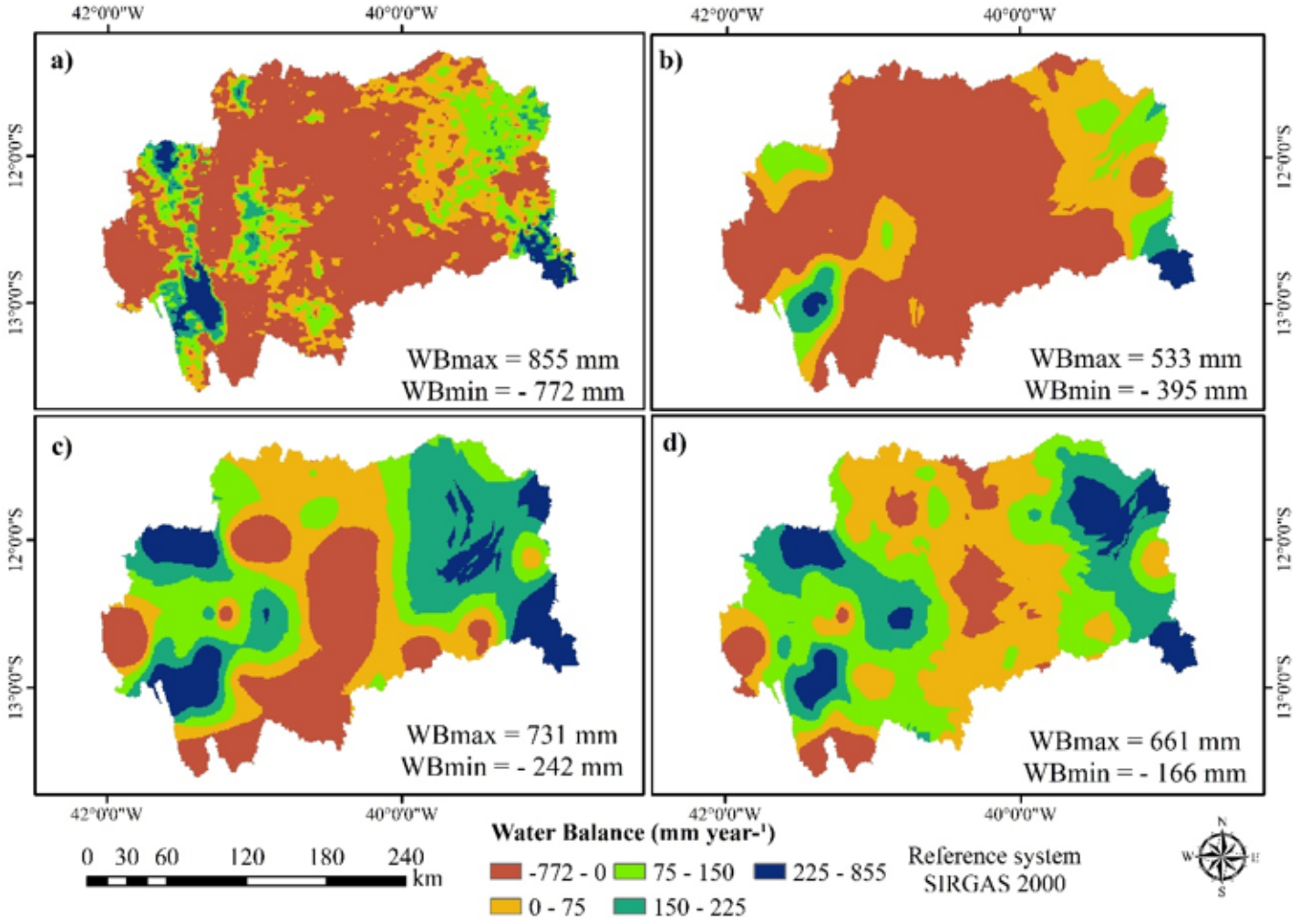

Figure 8

Water balance obtained with the IDW precipitation and the ETR_{MOD16} (a), $ETR_{MOD16rsp}$ (b), ETR_{GLEAM} (c) and ETR_{TC} (d) for the Paraguaçu river watershed. WBmax corresponds to the maximum value of WB for each source and WBmin corresponds to the minimum value of WB for each source

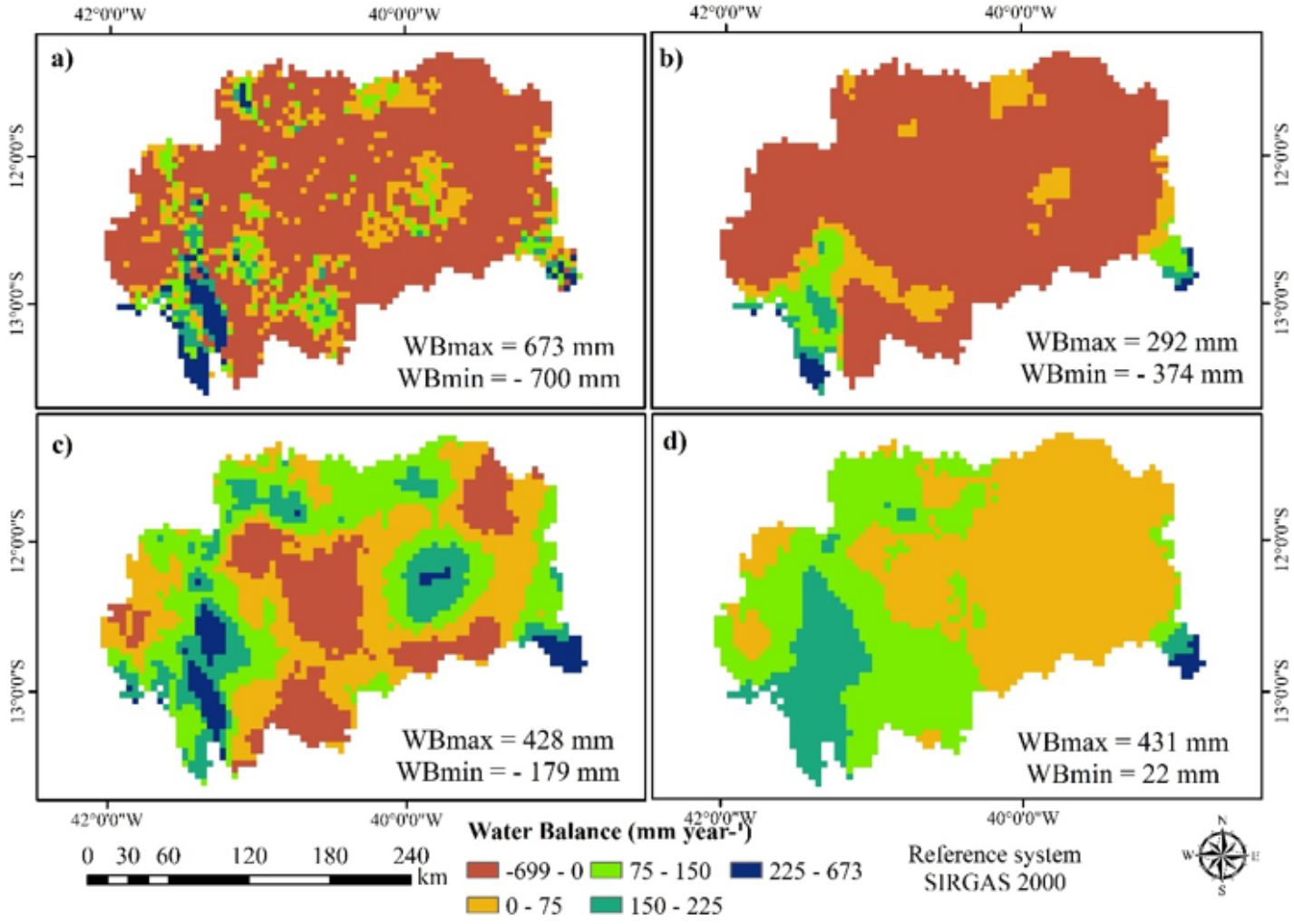

Figure 9

Water balance obtained with the TerraClimate precipitation and the ETR_{MOD16} (a), $ETR_{MOD16rsp}$ (b), ETR_{GLEAM} (c) and ETR_{TC} (d) for the Paraguaçu river watershed. WBmax corresponds to the maximum value of WB for each source and WBmin corresponds to the minimum value of WB for each source